Articles

Nanosheet Seed-Layer Assists Oriented Growth of Highly Luminescent Perovskite Films

Hiroyuki Tetsuka,[†] Hiroshi Takashima,*[,‡] Keiichi Ikegami,[§] Hiroshi Nanjo,[†] Takeo Ebina,*[,†] and Fujio Mizukami[†]

Research Center for Compact Chemical Process, National Institute of Advanced Industrial Science and Technology (AIST), 4-2-1 Nigatake, Sendai, Miyagi 983-8551, Japan, Nanoelectronics Research Institute, AIST, 1-1-1 Umezono, Tsukuba, Ibaraki 305-8568, Japan, and Nanotechnology Research Institute, AIST, 1-1-1 Umezono, Tsukuba, Ibaraki 305-8568, Japan

Received October 13, 2008. Revised Manuscript Received November 4, 2008

Oxide phosphors are attractive materials for various applications in optoelectronic devices due to their high chemical stability and efficient luminescent characteristics. As yet, however, the fabrication of high-quality luminescent thin films on a glass substrate remains challenging for practical implementation. Here, we report the efficient fabrication of highly oriented luminescent perovskite oxide films on a glass substrate using a monolayer film of oxide nanosheets as the seed layer. A densely packed monolayer film of $Ca_2Nb_3O_{10}$ nanosheets was prepared by the Langmuir−Blodgett (LB) method, where hybridization of the cationic molecules and the $Ca_2Nb_3O_{10}$ nanosheets produced stable LB films with large-area processability. Oriented thin films with a sharp and intense emission of $Pr_{0.002}(Ca_{0.6}Sr_{0.4})_{0.997}TiO_3$ were successfully obtained on a glass substrate modified with a seed layer. Highly luminescent transparent films are producible on inexpensive noncrystalline substrates; this approach also enables large-area processing of high-quality thin-film phosphors.

Introduction

Oxide thin-film phosphors are of great interest for various prospective applications in field-emission displays and electroluminescent devices because oxide phosphors present possible advantages of high chemical stability and efficient luminescent characteristics.[1] Among oxide phosphors of various types, the recent development of perovskite-type oxide phosphors has been revitalized through discovery of intense emissions from several materials. The Pr^{3+}-doped titanates $ATiO_3$ (A = Ca, Sr, Ba) and $Sr_{n+1}Ti_nO_{3n+1}$ (n = 1, 2, ∞) are reported as potential red phosphors.[2−4] Actually, $SrHfO_3$:Tm^{3+} has been proposed as a blue phosphor.[5] Furthermore, intense luminescence of several colors has been found in alkaline-earth stannate systems.[6,7] Preparation of transparent thin films on a glass substrate is desirable to apply these materials to practical optoelectronic devices. One limitation in thin-film forms is their low luminescent intensity compared to bulk powders. Optical confinement of the light because of planar interfaces and poor crystallinity is generally inferred as the primary cause of low emission intensity. Control of film orientations and particle sizes will be a key technology to obtain high luminescence properties and transparency because these properties are strongly influenced by their crystallinity, crystallographic orientations, and texture.[8,9] An ideal method to control film orientation is epitaxial growth on a lattice-matched single crystal substrate. However, size limitations and high cost of single crystals have hampered their practical implementation. Herein, we describe the efficient fabrication of oriented luminescent perovskite films on a glass substrate using a monolayer film of oxide nanosheets. Highly luminescent transparent perovskite films are producible on inexpensive noncrystalline substrates; this approach also enables large-area processing of high-quality thin-film phosphors.

Recently, layered inorganic materials such as layered transition-metal oxides and smectite clay minerals have

* To whom correspondence should be addressed. E-mail: h-takashima@asit.go.jp (H.T.), takeo-ebina@aist.go.jp (T.E.).
[†] Research Center for Compact Chemical Process.
[‡] Nanoelectronics Research Institute.
[§] Nanotechnology Research Institute.

(1) Yen, W. M.; Shionoya, S.; Yamamoto, H. *Phosphor Handbook*; CRC Press: New York, 2006.
(2) Okamoto, S.; Yamamoto, H. *Appl. Phys. Lett.* **2001**, *78*, 655–657.
(3) Kyomen, T.; Sakamoto, R.; Sakamoto, N.; Kunugi, S.; Itoh, M. *Chem. Mater.* **2005**, *17*, 3200–3204.
(4) Inaguma, Y.; Nagasawa, D.; Katsumata, T. *Jpn. J. Appl. Phys.* **2005**, *44*, 761–764.
(5) Yamamoto, H.; Mikami, M.; Shimomura, Y.; Oguri, Y. *J. Lumin.* **2000**, *87−89*, 1079–1082.
(6) Mizoguchi, H.; Woodward, P. M.; Park, C.-H.; Keszler, D. A. *J. Am. Chem. Soc.* **2004**, *126*, 9796–9800.
(7) Ueda, K.; Maeda, T.; Nakayashiki, K.; Goto, K.; Nakachi, Y.; Takashima, H.; Nomura, K.; Kajihara, K.; Hosono, H. *Appl. Phys. Exp.* **2008**, *1*, 015003–015005.
(8) Takashima, H.; Ueda, K.; Itoh, M. *Appl. Phys. Lett.* **2006**, *89*, 261915–261917.
(9) Lee, Y. E.; Norton, D. P.; Budai, J. D. *Appl. Phys. Lett.* **1999**, *74*, 3155–3157.

10.1021/cm8027912 CCC: $40.75
Published on Web 12/05/2008

attracted much attention as inorganic units to construct various nanostructures because of their unique intercalation and exfoliation properties.[10−13] They can be delaminated to a 1-nm-thick nanosheet with high in-plane strength, high stiffness, and a high aspect ratio. An attractive aspect of the exfoliated nanosheets is their high crystallinity inherited from layered precursors: an individual nanosheet can be considered as a two-dimensional single crystal. Schaak et al. and Muramatsu et al. reported fabrication of a densely packed monolayer film of $Ca_2Nb_3O_{10}$ nanosheets on a glass substrate via the different approaches, such as chemical adsorption and Langmuir−Blodgett (LB) technique, from the colloidal suspension obtained by delamination of layered perovskite oxide $KCa_2Nb_3O_{10}$.[14,15] The extremely flat and dense monolayer film prepared by LB method was used as a seed layer to control crystal growth.[16] Oriented thin films of lattice-matched $SrTiO_3$ and TiO_2 were obtained using a monolayer film of $Ca_2Nb_3O_{10}$ nanosheets as the seed layer. Presumably, this method is expandable to fabrication of high-quality perovskite oxide phosphors on a glass substrate, thereby producing highly luminescent films. Although densely packed monolayer films of $Ca_2Nb_3O_{10}$ nanosheets have been prepared with no amphiphilic additives at suspension concentrations of ca. 0.08 g L^{-1}, it is difficult to deposit a large continuous film because of the low capability of flowing of a monolayer film of $Ca_2Nb_3O_{10}$ nanosheets. In this work, we examined fabrication of a $Ca_2Nb_3O_{10}$ nanosheet seed layer using hybridization of amphiphilic molecules and $Ca_2Nb_3O_{10}$ nanosheets, which engenders stable Langmuir films because of van der Waals interactions between the alkyl chains in amphiphilic molecules. This hybridization also reduces the suspension concentration through enhanced adsorption of nanosheets to the air−water interface derived from electrostatic interaction between the amphiphilic molecules and nanosheets.

Experimental Section

Preparation of $Ca_2Nb_3O_{10}$ Nanosheet Suspension. A monodisperse colloidal nanosheet of $Ca_2Nb_3O_{10}$ was prepared by delaminating $KCa_2Nb_3O_{10}$. The starting material $KCa_2Nb_3O_{10}$ was prepared through solid-state reaction of K_2CO_3, $CaCO_3$, and Nb_2O_5 at 1200 °C for 12 h in air. Interlayer cations were converted into protons through acid exchange with 5 M HNO_3. This protonation was repeated three times by exchanging nitric acid solution. The resulting $HCa_2Nb_3O_{10}\cdot 1.5H_2O$ was reacted with an aqueous solution containing the same concentration of tetrabutylammonium hydroxide (TBAOH), which induced delamination into unilamellar nanosheets ($TBA_x[H_{1-x}Ca_2Nb_3O_{10}\cdot 1.5H_2O]$).

Fabrication of the Seed Layer on a Glass Substrate. Quartz glass was used as a substrate. Monolayer films of $Ca_2Nb_3O_{10}$ nanosheet−DOA hybrid were fabricated using the Langmuir−Blodgett deposition method with dioctadecyldimethylammonium bromide (DOA) as amphiphilic molecules. A diluted colloidal suspension (ca. 0.008 g L^{-1}) of the nanosheets was used as subphase and put in a Langmuir trough. Compression at a velocity of 5 cm^2 min^{-1} was performed on a Langmuir film balance and monitored by measurement of the surface pressure versus surface area (π−A) isotherms. Nanosheets were transferred onto the glass substrate using quasi-horizontal lifting method under 45 mN m^{-1} of surface pressure.

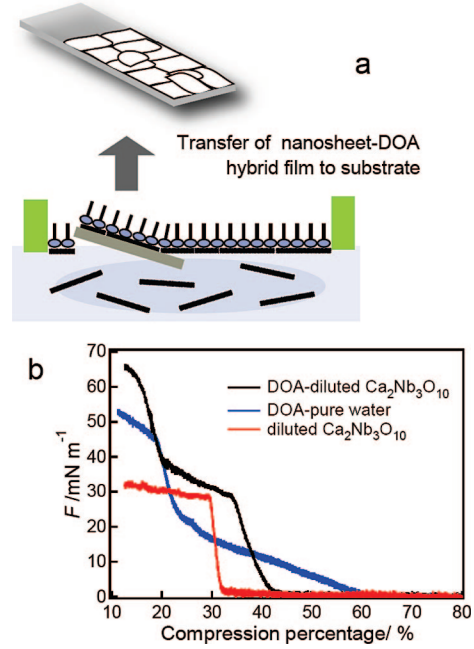

Figure 1. (a) Schematic explanation of deposition of $Ca_2Nb_3O_{10}$ nanosheet−DOA hybrid monolayer film using Langmuir−Blodgett method. (b) The π−A isotherms of DOA monolayers spread on the $Ca_2Nb_3O_{10}$ nanosheet suspension or pure water, and monolayer of $Ca_2Nb_3O_{10}$ nanosheets without DOA molecules. The x axis for the molecular area was converted to the percentage of surface area relative to the area before compression.

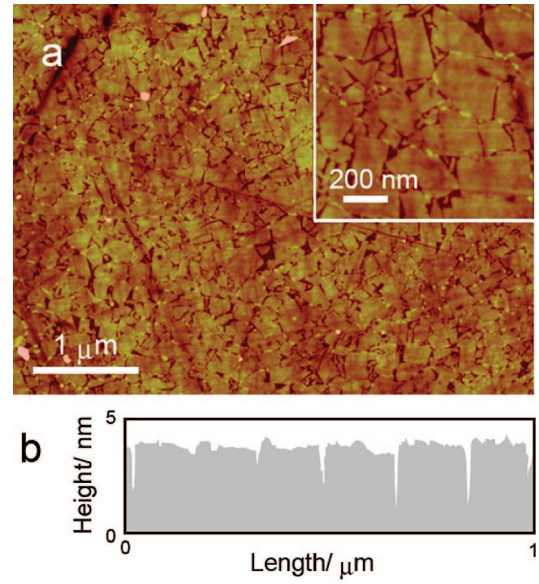

Figure 2. (a) AFM image of $Ca_2Nb_3O_{10}$ nanosheet−DOA hybrid film on a glass substrate. The inset shows the magnified image. (b) AFM height profile of the film.

Synthesis of $Pr_{0.002}(Ca_{0.6}Sr_{0.4})_{0.997}TiO_3$ Thin Films. $Pr_{0.002}(Ca_{0.6}Sr_{0.4})_{0.997}TiO_3$ thin films were grown using pulsed laser deposition

(10) Kuroda K.; Sasaki, T. *Science and Applications of Inorganic Nanosheets*; CMC Press: Tokyo, 2005.
(11) Tetsuka, H.; Ebina, T.; Mizukami, F. *Adv. Mater.* **2008**, *20*, 3039–3043.
(12) Tetsuka, H.; Ebina, T.; Nanjo, H.; Mizukami, F. *J. Mater. Chem.* **2007**, *17*, 3545–3550.
(13) Ebina, T.; Mizukami, F. *Adv. Mater.* **2007**, *19*, 24502–453.
(14) Schaak, R. E.; Mallouk, T. E. *Chem. Mater.* **2000**, *12*, 2513–2516.
(15) Muramatsu, M.; Kosho, K.; Ebina, Y.; Wang, K.; Sasaki, T.; Ishida, T.; Miyake, K.; Haga, M. *Langmuir* **2005**, *21*, 6590–6595.
(16) Shibata, T.; Fukuda, K.; Ebina, Y.; Kogure, T.; Sasaki, T. *Adv. Mater.* **2008**, *20*, 231–235.

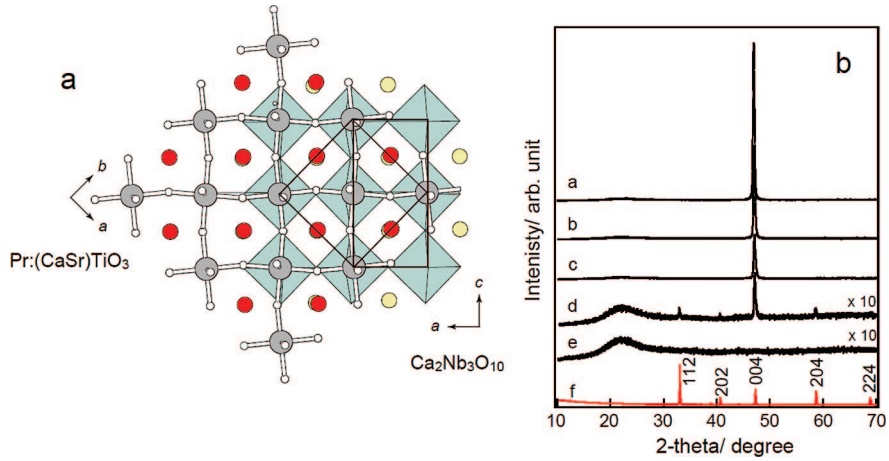

Figure 3. (a) Schematic illustration showing the epitaxial growth relation between the orthorhombic $Pr_{0.002}(Ca_{0.6}Sr_{0.4})_{0.997}TiO_3$ (001) and $Ca_2Nb_3O_{10}$ (010) planes. (b) XRD patterns for $Pr_{0.002}(Ca_{0.6}Sr_{0.4})_{0.997}TiO_3$ films grown on glass with (a−c: a, after 1000 °C annealing; b, after 800 °C annealing; c, as-grown) and without (d−e: d, after 800 °C annealing; e, as-grown) a nanosheet seed layer. All films were prepared using pulsed laser deposition. Indicated in red (f) is the simulated pattern of $Pr_{0.002}(Ca_{0.6}Sr_{0.4})_{0.997}TiO_3$ using the program Rietan-2000.[19] The atomic positions were set to those of $Ca_{0.75}Sr_{0.25}TiO_3$ having the same symmetry (Inorganic Crystal Structure Database (ICSD) #94569).

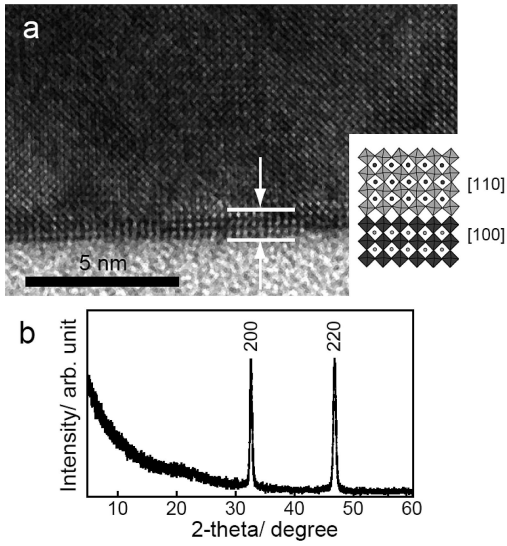

Figure 4. (a) Cross-sectional HRTEM image of a $Pr_{0.002}(Ca_{0.6}Sr_{0.4})_{0.997}TiO_3$ thin film grown on glass with a nanosheet seed layer taken from the $Pr_{0.002}(Ca_{0.6}Sr_{0.4})_{0.997}TiO_3$ [110] direction. (b) In-plane XRD pattern of $Pr_{0.002}(Ca_{0.6}Sr_{0.4})_{0.997}TiO_3$ film on a glass substrate with a nanosheet seed layer.

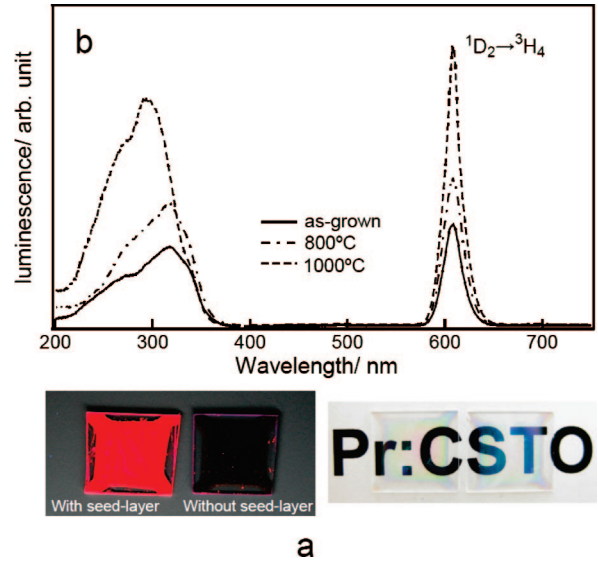

Figure 5. (a) The left image shows emissions from as-grown $Pr_{0.002}(Ca_{0.6}Sr_{0.4})_{0.997}TiO_3$ thin films on a glass substrate with (left) and without (right) a seed layer, with excitation using an ultraviolet lamp (254 nm). An optical image of the films after thermal annealing (1000 °C) is shown at the right. (b) Excitation spectra monitored at 610 nm (left) and emission spectra (right) of the $Pr_{0.002}(Ca_{0.6}Sr_{0.4})_{0.997}TiO_3$ films grown on glass with a nanosheet seed layer as functions of annealing temperature.

with a ceramic $Pr_{0.002}(Ca_{0.6}Sr_{0.4})_{0.997}TiO_3$ polycrystalline target. During film growth, the glass substrate with a $Ca_2Nb_3O_{10}$ nanosheet−DOA hybrid was heated to ca. 600 °C. The oxygen partial pressure was controlled at 10 Pa. An ArF excimer laser (λ = 193 nm) was used with a repetition rate of 8 Hz and a fluence of 1.2 J cm^{-2} $pulse^{-1}$ at the target surface. Sol−gel films were prepared using the following procedure. A precursor solution was prepared from calcium acetate, strontium acetate, titanium isopropoxide (TiIP), and praseodymium isopropoxide (PrIP). Acetic acid was used as a solvent, and acetylacetone (AcAc) was added as a stabilizer. Calcium acetate and strontium acetate were initially dissolved in acetic acid under constant stirring to yield a transparent solution. Then TiIP mixed with AcAc (molar ratio of Ti:AcAc = 1:1) was added to the acetate solution. Finally, PrIP was added to the mixed solution. The obtained clear solution was stirred continuously for 12 h in a closed flask; then methanol was added as a final setup to obtain 0.3 M solution. The precursor sol was applied by spin coating onto glass substrate modified with a seed layer at 5000 rpm for 30 s. After coating, the films were dried at 120 °C on a hot plate for 1 min and were then heated at 1000 °C for 1 h.

Instrumentation. The crystal structure and phase of the films were characterized using X-ray diffractometry (XRD, MXP18; Mac Science Ltd.) with a Cu K_a source under an applied voltage of 40 kV and a current of 250 mA. In-plane XRD measurements were performed using grazing incidence X-ray scattering (ATX-G; Rigaku Corp.). The surface roughness and morphology of the films were investigated using an atomic force microscope (AFM, NanoScopeIIIa; Veeco Instruments). Subsequently, HRTEM observations were carried out using a transmission electron microscope (HF-2000; Hitachi Ltd.) operating at an accelerating voltage of 200 kV. The cross-sectional TEM specimen was prepared using Ar ion milling. Fluorescence spectra were recorded using a spectrofluorometer (F-4500; Hitachi Ltd.) with excitation at 254 nm (450 W Xe lamp). In addition, optical transmittance and reflectance in the visible region of the films were recorded using a spectrophotometer

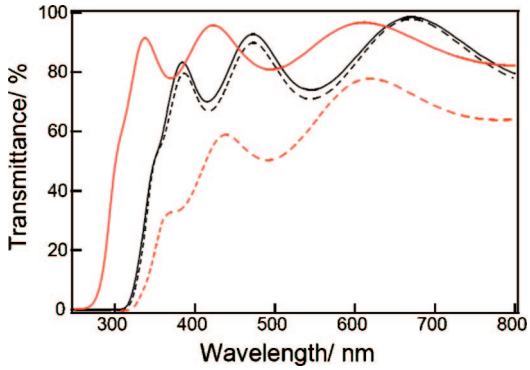

Figure 6. Transmission spectra of the $Pr_{0.002}(Ca_{0.6}Sr_{0.4})_{0.997}TiO_3$ films grown with (black) or without (red) a seed layer. Solid lines are as-grown films; broken lines are annealed films (1000 °C).

(UV/vis/NIR, V570; Jasco Inc.). The reflectance was measured at an incident angle of 5° using an additional attachment (SLM-508).

Results and Discussion

Figure 1a presents a preparation strategy for fabricating a closely packed monolayer film of $Ca_2Nb_3O_{10}$ nanosheet on a glass substrate using a positively charged monolayer of dioctadecyldimethylammonium bromide (DOA) as amphiphilic molecules. The colloidal suspension of $Ca_2Nb_3O_{10}$ nanosheets, whose concentration was adjusted to 0.008 g L^{-1}, was used as a subphase under the DOA monolayers. The surface pressure versus surface area ($\pi-A$) isotherms (Figure 1b) shows that hybridization of the $Ca_2Nb_3O_{10}$ nanosheets with the DOA monolayer creates a stable monolayer film. The low collapse pressure (30 mN m^{-1}) is a manifestation of an unstable $Ca_2Nb_3O_{10}$ monolayer formation on the subphase without the amphiphilic molecules. On the other hand, a stable $Ca_2Nb_3O_{10}$ nanosheet−DOA hybrid monolayer, with a pronounced condensed phase and a collapse pressure of ca. 65 mN m^{-1}, was formed on the air−water interface. The plateau region at ca. 30 mN m^{-1} results from a phase transition occurring from the perpendicular alignment of alkyl chains in DOA molecules. Cationic DOA molecules are expected to contribute to stabilization of the monolayer film of anionic $Ca_2Nb_3O_{10}$ nanosheets. The high collapse pressure offers efficient transfer of Langmuir films to substrates. Densely packed $Ca_2Nb_3O_{10}$ nanosheet−DOA hybrid films were prepared by compressing the monolayer at a surface pressure of 45 mN m^{-1} and then transferred to the glass substrate using the quasi-horizontal lifting method. An atomic force microscopy (AFM) image of a monolayer film of the $Ca_2Nb_3O_{10}$ nanosheet−DOA hybrids is presented in Figure 2a. The $Ca_2Nb_3O_{10}$ nanosheets covered nearly 95% of the glass surface; overlapping of the $Ca_2Nb_3O_{10}$ nanosheets was minimized. The film thickness estimated from gaps between nanosheets was ca. 4.0 nm (Figure 2b), which is close to the sum of the crystallographic thickness of unilamellar $Ca_2Nb_3O_{10}$ nanosheet (ca. 1.5 nm) and DOA molecule (ca. 2.4 nm). The root-mean-square roughness value (R_a) was estimated as 0.33 nm. Consequently, the homogeneous monolayer film was prepared by hybridization of the DOA molecules and the $Ca_2Nb_3O_{10}$ nanosheet. Formation of a large continuous $Ca_2Nb_3O_{10}$ nanosheet−DOA hybrid film was also confirmed from results of the multilayer deposition test (Figure S1, Supporting Information).

We investigated the oriented growth of perovskite oxide phosphor $Pr_{0.002}(Ca_{0.6}Sr_{0.4})_{0.997}TiO_3$ on a glass substrate modified with a monolayer film of $Ca_2Nb_3O_{10}$ nanosheets as a seed layer, using pulsed-laser deposition. The $Pr_{0.002}(Ca_{0.6}Sr_{0.4})_{0.997}TiO_3$ crystallized in an orthorhombic structure belonging to the space group *Pbnm* (a = 0.5456 nm, b = 0.5462 nm, c = 0.7718 nm).[17] Actually, $KCa_2Nb_3O_{10}$ has the same structure system but its space group is different (*Cmcm*: a = 0.3882 nm, b = 2.951 nm, c = 0.7714 nm).[18] Figure 3a shows the epitaxial growth relation between the $Pr_{0.002}(Ca_{0.6}Sr_{0.4})_{0.997}TiO_3$ (001) and $KCa_2Nb_3O_{10}$ (010) planes, as estimated from consideration of the symmetries in space groups *Pbnm* and *Cmcm*: 45° rotated $Pr_{0.002}(Ca_{0.6}Sr_{0.4})_{0.997}TiO_3$ cell is grown on a $a\sqrt{2} \times c\sqrt{2}/2$ $Ca_2Nb_3O_{10}$ square cell. The expected lattice mismatch is expected to be <0.3% when the $Pr_{0.002}(Ca_{0.6}Sr_{0.4})_{0.997}TiO_3$ film is grown using this configuration. Figure 3b shows X-ray diffraction (XRD) patterns of $Pr_{0.002}(Ca_{0.6}Sr_{0.4})_{0.997}TiO_3$ films grown on glass substrates with and without a seed layer. During film growth, the glass substrate was heated to ca. 600 °C. Heat treatments were performed at 800 or 1000 °C in air for 2 h. The film thickness was typically ca. 300 nm. For films grown with a seed layer, only one intense diffraction peak was observed at $2\theta = 47.0°$, which can be assigned as that of a $Pr_{0.002}(Ca_{0.6}Sr_{0.4})_{0.997}TiO_3$ (004) reflection. Because the annealing temperature increased, the peak became more intense and sharp (full widths at half-maximum (fwhm) decreased from 0.36° to 0.29°), indicating that the crystallinity of the films improved with the annealing temperature. The fwhm of the (004) rocking curve was ca. 0.13° for the film annealed at 1000 °C, suggesting a high degree of *c*-axis preferred orientation. On the other hand, no diffraction peak was observed from the as-grown film deposited without a seed layer, although it was crystallized by annealing at temperatures greater than 700 °C. Several diffraction peaks with indices of 112, 202, 004, and 204 were discernible, which is consistent with expectations for a randomly oriented polycrystalline $Pr_{0.002}(Ca_{0.6}Sr_{0.4})_{0.997}TiO_3$. These results indicate that the monolayer of $Ca_2Nb_3O_{10}$ nanosheets can induce oriented growth of $Pr_{0.002}(Ca_{0.6}Sr_{0.4})_{0.997}TiO_3$ film.

Figure 4a presents a cross-sectional high-resolution transmission electron microscopy (HRTEM) image of as-grown $Pr_{0.002}(Ca_{0.6}Sr_{0.4})_{0.997}TiO_3$ film on a glass substrate with a $Ca_2Nb_3O_{10}$ nanosheet seed layer. The highly crystalline $Pr_{0.002}(Ca_{0.6}Sr_{0.4})_{0.997}TiO_3$ was grown along the [001] direction, as expected from XRD analysis, which is perpendicular to the substrate. A unilamellar nanosheet, which was ca. 1.5 nm thick, was observable between the $Pr_{0.002}(Ca_{0.6}Sr_{0.4})_{0.997}TiO_3$ film and glass substrate. The interface was clear and clean; no signs of interfacial reactions were observed. This confirms the epitaxial growth of $Pr_{0.002}(Ca_{0.6}Sr_{0.4})_{0.997}TiO_3$ on individual $Ca_2Nb_3O_{10}$ nanosheets. It is also implied that the DOA used as amphiphilic molecules only slightly affects the crystal growth or crystallinity of $Pr_{0.002}(Ca_{0.6}Sr_{0.4})_{0.997}TiO_3$

(17) Qin, S.; Becerro, A. I.; Seifert, F.; Gottsmann, J.; Jiang, J. *J. Mater. Chem* **2000**, *10*, 1609–1615.
(18) Fukuoka, H.; Isami, T.; Yamanaka, S. *J. Solid State Chem.* **2000**, *151*, 40–45.
(19) Izumi, F.; Ikeda, T. *Mater. Sci. Forum* **2000**, *321−324*, 198–203.

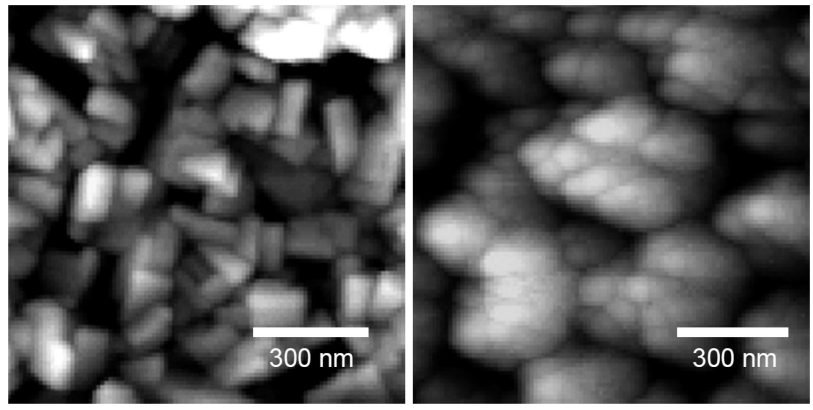

Figure 7. AFM images of the annealed $Pr_{0.002}(Ca_{0.6}Sr_{0.4})_{0.997}TiO_3$ films on glass substrates with (left) and without (right) a seed layer.

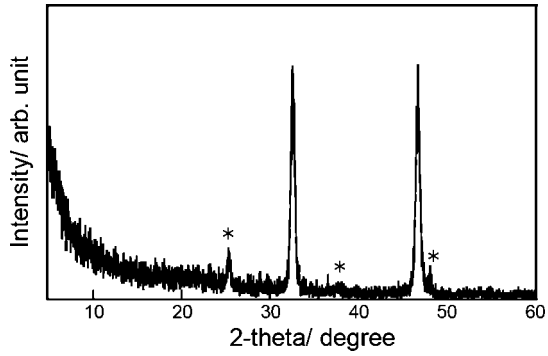

Figure 8. In-plane XRD of the $Pr_{0.002}(Ca_{0.6}Sr_{0.4})_{0.997}TiO_3$ films grown on a glass substrate modified with a seed layer after thermal annealing (1000 °C). The peaks (*) are ascribed to the impurity phase TiO_2 (anatase, International Centre for Diffraction Data (ICDD) #01-070-7348).

films. Because the nanosheets of several micrometers in lateral size are tiled randomly in the azimuthal direction on the substrates, the $Pr_{0.002}(Ca_{0.6}Sr_{0.4})_{0.997}TiO_3$ film is expected to have macroscopically uniaxial orientation. Figure 4b depicts the in-plane XRD pattern of the $Pr_{0.002}(Ca_{0.6}Sr_{0.4})_{0.997}TiO_3$ films. The film exhibited two sharp diffraction peaks at 32.6 and 46.8°, which can be indexed to 200 and 220. The absence of general *hkl* peaks was consistent with a uniaxial orientation of the film, which suggests that the grown crystals have a random in-plane direction.

Luminescence and optical properties of oxide thin-film phosphors are closely correlated with their crystallinity, crystal orientation, and surface morphology. The emission image of as-grown $Pr_{0.002}(Ca_{0.6}Sr_{0.4})_{0.997}TiO_3$ films on a glass substrate with (left) and without (right) a seed layer is shown at the left of Figure 5a. The film grown with a seed layer shows a strong red emission under irradiation using a UV-lamp of 254 nm. On the other hand, film grown without a seed layer shows no light emission, perhaps because of its low crystallinity. In Figure 5b, we show excitation spectra monitored at 610 nm (left) and emission spectra excited by 254 nm light (right) for $Pr_{0.002}(Ca_{0.6}Sr_{0.4})_{0.997}TiO_3$ films grown with a seed layer as functions of annealing temperature. A sharp emission peak was observed at 610 nm. The emission is assigned to $4f^2-4f^2$ transition of Pr^{3+} ions from the excited state $^1D_2$ to the ground state $^3H_4$.[20] The energy transfer occurs from photoexcited carriers in $Pr_{0.002}(Ca_{0.6}Sr_{0.4})_{0.997}TiO_3$ to Pr^{3+} via 4f5d transition, resulting in the red luminescence. It is readily apparent that the emission intensity increases with increasing annealing temperature. The emission peaks become sharper: FWHMs decrease from 21 to 18 nm, indicating that the symmetry around Pr^{3+} ions is enhanced through improved crystallinity, as suggested by results of XRD analysis. The excitation spectra show three peaks at approximately 335, 315, and 270 nm. These peaks are assigned, respectively, to the excited states of Pr^{3+} ions, the electronic transitions from O 2p to Ti 3d states in $Pr_{0.002}(Ca_{0.6}Sr_{0.4})_{0.997}TiO_3$, and the 4f5d transitions of Pr^{3+} ions. The excitation peak around 315 nm shows a blue shift after high-temperature annealing. This phenomenon is not clearly understood at this point, as discussed below.

The transmittance spectra of the $Pr_{0.002}(Ca_{0.6}Sr_{0.4})_{0.997}TiO_3$ films on a glass substrate with and without a seed layer are depicted in Figure 6. The films are colorless; the average transmittance in the visible region (400−800 nm) is greater than 80% for the films grown with a seed layer. The visibility of the lettering through the film demonstrates its high optical transmittance (right image of Figure 5a). Note that the absorption of the $Ca_2Nb_3O_{10}$ nanosheet, which is 350 nm (band gap: 3.53 eV), is negligible compared to that of the $Pr_{0.002}(Ca_{0.6}Sr_{0.4})_{0.997}TiO_3$ film due to its thickness as thin as ca. 1.5 nm.[21] Transmittance spectra show some differences in the films grown with and without a seed layer, i.e., uniaxially oriented film and polycrystalline film. First, transmittance of the film grown without a seed layer was decreased drastically to 60% by thermal annealing. Subsequently, AFM measurements revealed large cauliflower-like clusters, of 200−500 nm diameter, formed in polycrystalline film, whereas oriented films comprise small rod-like particles of 70 × 120 nm diameter (Figure 7). Consequently, light scattering through the large clusters is assumed to be the predominant factor for transmittance reduction. The existence of grain boundaries and random grain alignment in polycrystalline films also engenders light scattering. Second, the absorption edge of the film grown without a seed layer markedly shifts to the longer wavelength region after thermal annealing. This shift is attributable to the structural change of film and transition from an amorphous to a polycrystalline

(20) Jia, W.; Xu, W.; Rivera, I.; Perez, A.; Fernandez, F. *Solid State Commun.* **2003**, *126*, 153–157.

(21) Compton, O. C.; Carroll, E. C.; Kim, J. Y.; Larsen, D. S.; Osterloh, F. E. *J. Phys. Chem. C* **2007**, *111*, 14589–14592.

phase.[22] On the other hand, the absorption edges of the oriented films remain at around 315 nm, although a slight red shift occurs. This behavior is somewhat contrary to the tendency that is apparent for the excitation spectra. In-plane XRD analysis revealed extra peaks to a depth of a few nanometers from the surface after high-temperature annealing (Figure 8), implying the formation of an impurity phase near the film surface. The existence of such an impurity phase is expected to cause the blue shift in the excitation spectrum. However, the impurity phase only slightly affects the luminescence because the form and position of the emission spectrum is fundamentally identical to those of other films. The above results show that the oriented films exhibit superior luminescence and optical properties compared to the polycrystalline films. These excellent properties are expected to promote the application of the oriented films.

Finally, we attempted to prepare the large-area oriented luminescent films on a glass substrate modified with a monolayer film of $Ca_2Nb_3O_{10}$ nanosheets. Here, we examined the fabrication of $Pr_{0.002}(Ca_{0.6}Sr_{0.4})_{0.997}TiO_3$ films using the sol−gel method, which is a more industrial film-fabrication technique. The $Pr_{0.002}(Ca_{0.6}Sr_{0.4})_{0.997}TiO_3$ films were fabricated on a glass substrate with a size of 10 × 36 mm. Sol−gel $Pr_{0.002}(Ca_{0.6}Sr_{0.4})_{0.997}TiO_3$ films appeared to have very similar properties as PLD films; no noticeable difference was recognized in the XRD pattern and emission spectrum. High *c*-axis orientation and luminescence properties were maintained on a large-area substrate (Figure S2, Supporting Information). It is also evident that a large continuous monolayer film of $Ca_2Nb_3O_{10}$ nanosheets was formed on a glass substrate.

Summary

In summary, we have demonstrated a method of fabricating high-quality luminescent perovskite oxide films on a glass substrate using a monolayer film of oxide nanosheets as the seed layer. Densely packed monolayer film of $Ca_2Nb_3O_{10}$ nanosheets was prepared using the LB technique, where hybridization of the DOA molecules and the $Ca_2Nb_3O_{10}$ nanosheets produced stable LB films with large-area processability. Oriented thin films of $Pr_{0.002}(Ca_{0.6}Sr_{0.4})_{0.997}TiO_3$ were obtained on a glass substrate using the seed layer. They showed sharply intense red luminescence and high optical transparency compared to the polycrystalline films. Regarding the application of the thin-film phosphors, these transparent films with sharp and intense emission are useful for applications in future optoelectronic devices such as displays and light-emitting devices. This film fabrication technique is also useful for other perovskite oxide phosphors.

Supporting Information Available: Surface area curve, emission image of sol−gel film, and in-plane XRD profile (PDF). This material is available free of charge from via the Internet at http://pubs.acs.org.

CM8027912

(22) Ma, J. H.; Huang, Z. M.; Meng, X. J.; Liu, S. J.; Zhang, X. D.; Sun, J. L.; Xue, J. Q.; Chu, J. H. *J. Appl. Phys.* **2006**, *99*, 033515–033519.